doi:10.2533/chimia.2019.239 Chimia 73 (2019) 239–244

What Can We Learn from First Principles Multi-Scale Models in Catalysis? The Role of the Ni/Al_2O_3 Interface in Water-Gas Shift and Dry Reforming as a Case Study

Lucas Foppa[§*a], Kim Larmier[b], and Aleix Comas-Vives[ac]

[§]SCS-Metrohm Award for best oral presentation in Catalysis Science & Engineering

Abstract: Computational first principles models based on density functional theory (DFT) have emerged as an important tool to address reaction mechanisms and active sites in metal nanoparticle catalysis. However, the common evaluation of potential energy surfaces for selected reaction steps contrasts with the complexity of reaction networks under operating conditions, where the interplay of adsorbate populations and competing routes at reaction conditions determine the most relevant states for catalyst activity and selectivity. Here, we discuss how the use of a multi-scale first principles approach combining DFT calculations at the atomistic level with kinetic models may be used to understand reactions catalyzed by metal nanoparticles. The potential of such an approach is illustrated for the case of Al_2O_3-supported Ni nanoparticle catalysts in the water-gas shift and dry reforming reactions. In these systems, both Ni nanoparticle (metal) as well as metal/oxide interface sites are available and may play a role in catalysis, which depends not only on the energy for critical reaction steps, as captured by DFT, but also on the reaction temperature and adsorbate populations, as shown by microkinetic modelling and experiments.

Keywords: Density functional theory · Metal/oxide interfaces · Microkinetic modeling · Supported metal nanoparticle catalysts

Lucas Foppa studied engineering at the Universidade Federal do Rio Grande do Sul (UFRGS) in Brazil and at the École Centrale Marseille in France. After a MSc in chemistry at UFRGS, he joined ETH Zürich for a PhD devoted to the first principles modelling of metal nanoparticle catalysis. He is currently a Swiss National Science Foundation post-doc fellow at the Theory Department of the Fritz-Haber Institute of the Max Planck Society in Germany.

1. First Principles Modelling of Nanoparticle Catalysis

Major industrial processes in chemistry are carried out in many instances with supported transition-metal nanoparticle (NP) catalysts.[1] Some examples are water-gas shift (WGS) and methane reforming used for hydrogen and syngas (CO/H_2) production, respectively, the Fischer-Tropsch synthesis of hydrocarbons and the Haber-Bosch process for ammonia production. Elucidating the detailed reaction mechanisms and associated surface active sites in NP catalysis, at the molecular level, is therefore crucial in order to rationalize macroscopic observations and to enable the rational design of catalysts with tunable activity and selectivity towards the desired products. In addition to experimental approaches to investigate reaction mechanisms and active sites on NP catalysts, the recent development of high performance computing and periodic density functional theory (DFT) methods to efficiently solve the electronic structure problem in solids and surfaces boosted the use of computational methods to address these questions, with the advantage of giving direct access to the underlying electronic structure at the atomistic level.[2]

The first principles computational approach to investigate reaction mechanisms on NP catalysis typically concentrates on the evaluation of potential energy surfaces (PESs) for key selected elementary steps of the reaction of interest (Fig. 1a.1), which are known, or more often assumed, to be rate and/or selectivity-determining. More specifically, DFT is used to determine the energy of reactants, intermediates and transition states (TSs) adsorbed on (slab) surface or NP models for the catalyst surface sites. The relevance of mechanisms is then discussed based on the energetics of the selected reaction steps. The most likely pathways are those involving not too weak nor too strong binding of key reaction intermediates (thermodynamic factor) and/or those associated to low-energy TSs with hence affordable energy barriers (kinetic factor). When the full catalytic cycle can be evaluated by DFT, the energy span model, well established for homogeneous catalysis, is also often applied.[3] The energy span, which is generally the difference between the highest and lowest energy points of the PES, integrates both the thermodynamic and kinetic criteria (Fig. 1a.2) and could, in principle, be used as an indicator of the turnover frequency (TOF) and thus of the relevance associated to a given reaction route: the lower the reaction span is, the higher the TOF should be.

*Correspondence: Dr. L. Foppa[a]
E-mail: foppa@inorg.chem.ethz.ch
[a]Department of Chemistry and Applied Biosciences, ETH Zurich, Vladimir-Prelog-Weg 1–5, CH-8093 Zurich
[b]IFP Energies Nouvelles, Rond-Point de l'échangeur de Solaize, BP3, 69360 Solaize, France
[c]Current address: Department of Chemistry, Universitat Autònoma de Barcelona, 08193 Cerdanyola del Vallès, Catalonia, Spain

Nevertheless, it is not straightforward to know how selected parts of the PES or even how the PES of the full catalytic cycle relates to the overall activity or selectivity of the catalyst, since the actual *rates* of elementary steps during the reaction depend not only on the energetics of the process, but also on the concentration of reaction intermediates, which in the case of surface reactions corresponds to adsorbates populations or coverages (Fig. 1b.1). As a consequence, reaction intermediates and TSs whose energy actually affect the overall (observed) reaction rate and selectivity depend on the relative population of surface species and on the preferred reaction routes, which may be hard to infer based solely on examining PESs since they are sensitive to reaction conditions, for instance temperature, pressure and chemical potential of the gas-phase. In particular, surface sites may be poisoned or inhibited by the strong adsorption of reaction intermediates during the reaction, suppressing the rate for important reaction steps. Furthermore, even if PESs are drawn as a linear succession of elementary steps occurring in a determined sequence, in most cases several intermediates are part of multiple competing routes within very complex reaction networks (Fig. 1b.2) whose interplay is difficult to assess from reaction energy diagrams. This may be especially the case when multiple reaction sites are available (*e.g.* NP terraces, defects as well as support and NP/support interface sites) and reaction intermediates may migrate from one type of site to another.

The use of kinetic models derived from DFT calculations (also known as microkinetic models) applied to NP catalysis is an alternative to tackle the complexity of reaction networks under reaction conditions, since the contribution of adsorbate population is introduced into the calculated rate in addition to the energetic term provided by DFT and all reactions in the network are considered simultaneously.[4] Within microkinetic models, the electronic energy of surface species obtained from DFT combined with statistical mechanics for the estimation of Gibbs free-energies (*via* partition functions) is used to compute the reaction rates of all the elementary steps of the reaction network at reaction conditions (temperature and pressure). The gas-phase concentrations and coverages of adsorbed species are then explicitly determined by solving a system of differential equations describing the evolution of reaction rates in a model reactor, whose boundary conditions are the feed compositions (Fig. 2).[5] The interplay of all the elementary steps included in the microkinetic model with the reaction conditions determines the composition of adsorbed species and major reaction pathways, which in turn affect the catalyst activity (conversion) and selectivity.

Contrary to the analysis of the PESs for selected reaction steps, no assumption needs to be made regarding the intermediate(s) or TS(s) that control activity and selectivity when a microkinetic model is available. Instead, sensitivity analyses[6] can be performed to identify surface species whose stability affect the overall reaction rate or selectivity. The degree of rate control (DRC) analysis proposed by Campbell, for instance, identifies rate-determining steps (RDS) based on the evaluation of the degree of rate control quantity ($X_{RC,i}$)[6b] for each elementary step of the reaction network. $X_{RC,i}$ is the relative increase in the overall reaction rate that is obtained if the reaction rate constant for the elementary step i is increased infinitesimally, while keeping the reaction rate constants and the thermodynamic equilibrium constants for all the other elementary steps fixed. A positive (resp. negative) $X_{RC,i}$ value indicates that increasing the rate of the step i results in global reaction rate enhancement (resp. suppression). The elementary step i is said to be rate-determining (RDS) if $X_{RC,i} > 0$ or inhibitive if $X_{RC,i} < 0$, while zero DRC values indicate non-RDSs, *i.e.* steps whose

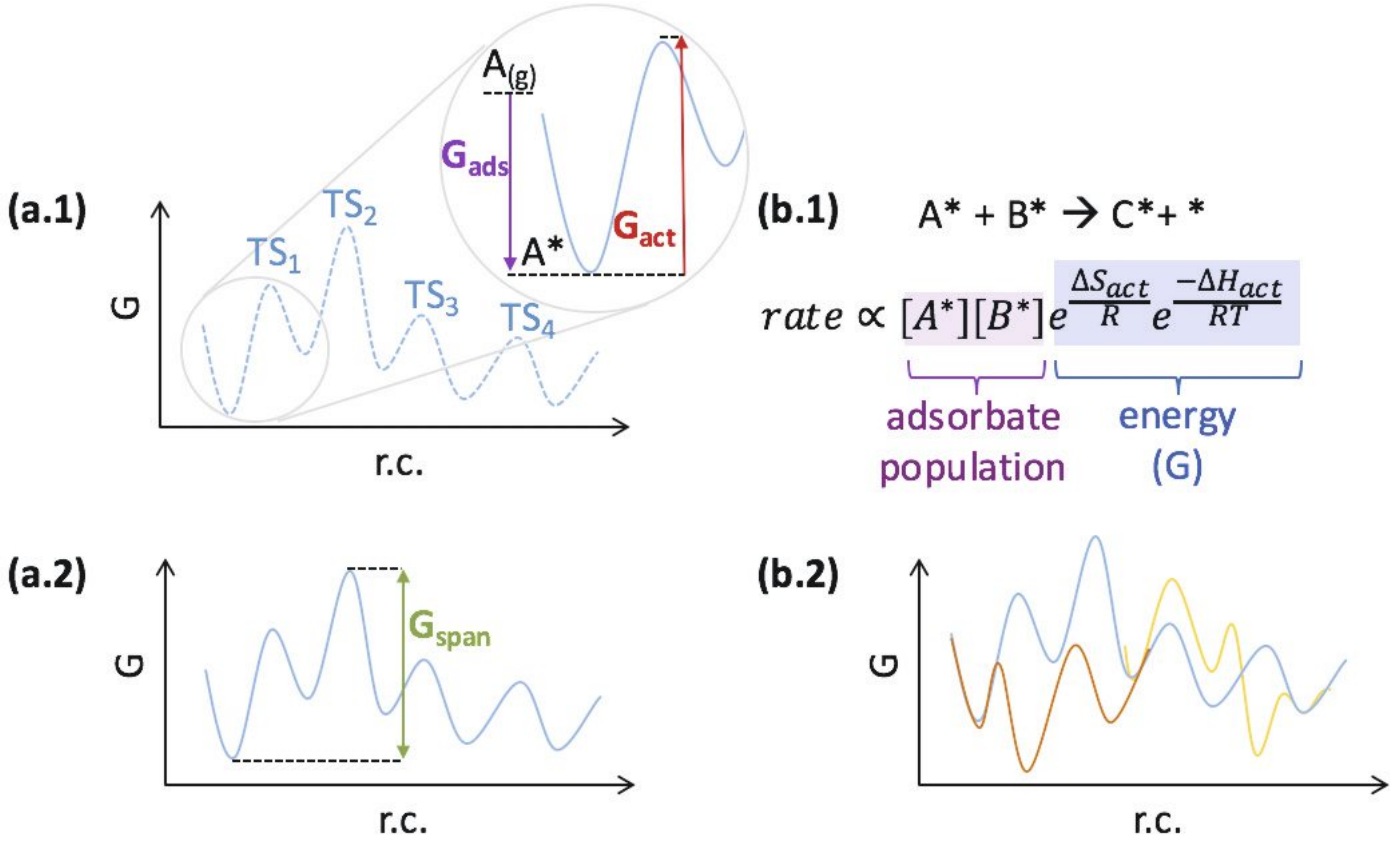

Fig. 1. (a) Common approaches to address reaction mechanisms and active sites on NP catalysts using DFT calculations: (a.1) evaluation of PESs for selected reaction steps, focusing on the adsorption (Gibbs) free-energy (G_{ads}) of intermediates (adsorbed species denoted by A*) and activation free-energies (G_{act}) to achieve TSs and (a.2) Evaluation of free-energy span (G_{span}) of full catalytic cycles. (b) Limitations of PES analysis and span model: (b.1) the rate of surface reactions depends on adsorbate population (coverage of the reacting species) and (b.2) reaction networks typically display interconnected pathways, with common intermediates. In the figure, G corresponds to Gibbs free-energy, r.c. (reaction coordinate) to an arbitrary reaction coordinate, ΔS_{act} and ΔH_{act} to activation entropy and enthalpy, respectively, R to the universal constant of the gases and T to the temperature.

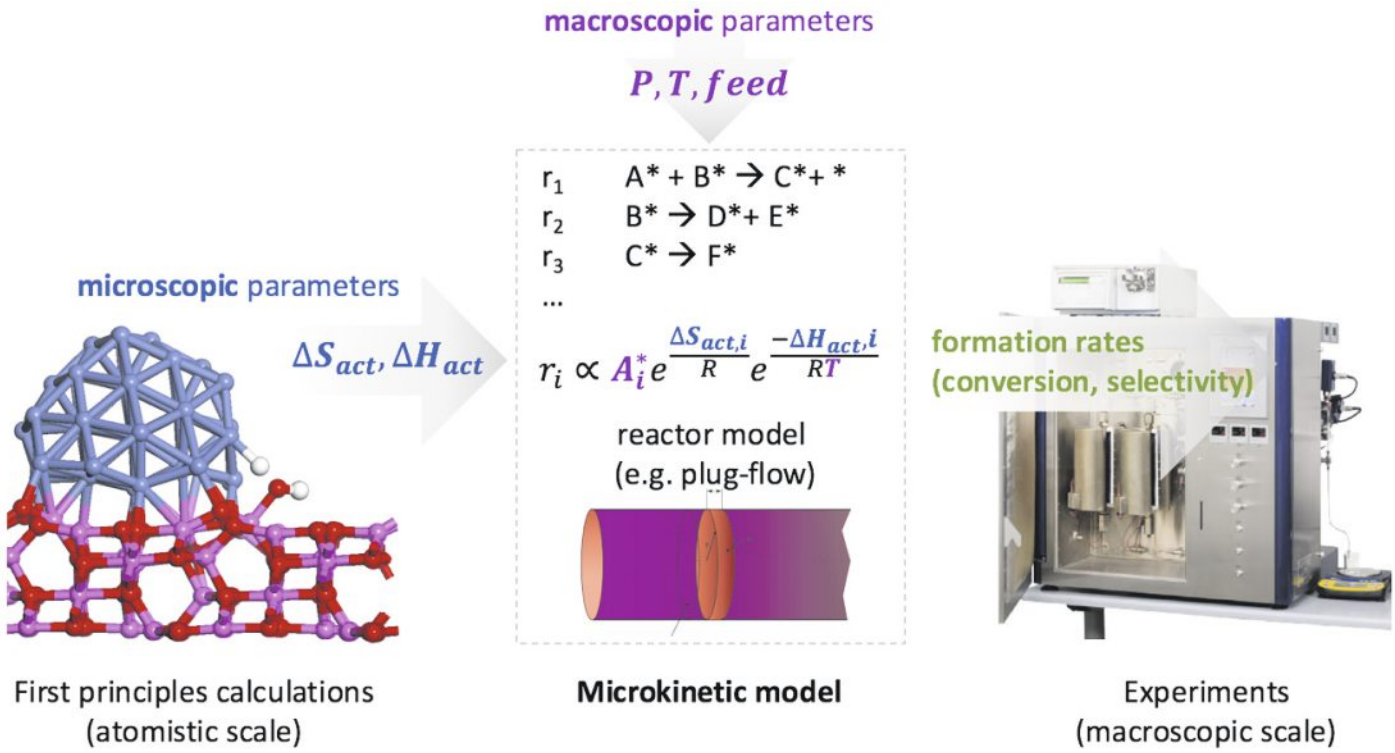

Fig. 2. Microkinetic models as a part of a multi-scale approach to link the atomistic (first principles calculations) with the macroscopic (experiments) scales. In the figure, ΔS_{act} and ΔH_{act} correspond to activation entropy and enthalpy for a given reaction elementary step, respectively, T to the temperature, P to the pressure, feed to the initial composition of reactants, r_i to the rate of the elementary surface reaction i, A_i^* to the coverage of adsorbates taking part in reaction i and R to the universal constant of the gases.

infinitesimal rate increase do not impact the global reaction rate. Similarly, a degree of thermodynamic rate control $X_{TRC,i}$ can be evaluated to identify reaction intermediates whose stability affect the overall rate.[6d] The DRC analysis is thus equivalent to the introduction of infinitesimal perturbations to the energy of each TS or intermediate of a given reaction network while monitoring changes on the outcome of the reaction, *i.e.* the conversion, as illustrated in Fig. 3. The information obtained from a DRC analysis is valuable for catalyst design, since it directly shows which intermediate(s) and TS(s) need to be stabilized (or de-stabilized) for the desired effect on the overall rate and selectivity. Indeed, the use of microkinetic models associated to DRC analysis has become standard in catalysts screening studies and also provided a broader mechanistic understanding for numerous reactions catalyzed by metal NPs as compared to the analysis of PESs alone.[4]

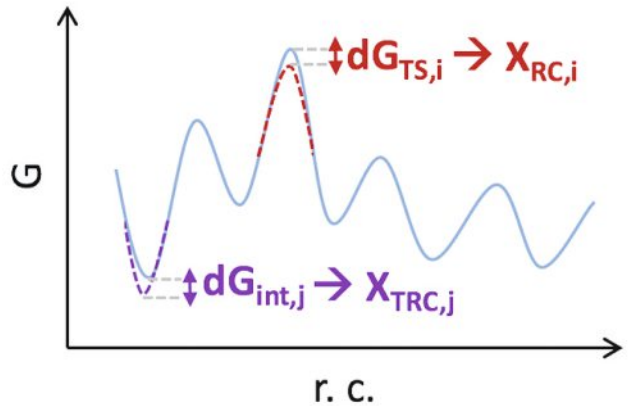

Fig. 3. DRC analysis pictured as infinitesimal perturbations to the Gibbs free-energy of each *i*-th TS and intermediate (int.) of the reaction network to evaluate the degree of rate control ($X_{RC,i}$) and degree of thermodynamic rate control ($X_{TRC,j}$) quantities, respectively, associated to each reaction step. In the figure, G corresponds to Gibbs free-energy and r.c. to an arbitrary reaction coordinate.

2. Ni/Al_2O_3 Interfaces in Water-Gas Shift and Dry Reforming of Methane

The combination of DFT calculations with microkinetic models provided a deeper understanding of the WGS (Eqn. (1)) and the dry reforming of methane (DRM, Eqn. (2)) reactions catalyzed by Ni NPs supported on alumina. The WGS is an important industrial technology for hydrogen production[7] and the DRM allows the transformation of natural gas into syngas (CO/H_2 mixture) in the industrially-relevant gas-to-liquid chain for the production of synthetic fuels,[8] being an interesting alternative to the commonly used steam reforming of methane which enables the conversion of CO_2 into value-added products.

$$CO_{(g)} + H_2O_{(g)} = CO_{2(g)} + H_{2(g)} \qquad \Delta_r H° = -41.1 kJ.mol^{-1} \quad (1)$$

$$CH_{4(g)} + CO_{2(g)} = 2\,H_{2(g)} + 2\,CO_{(g)} \qquad \Delta_r H° = 247.4\ kJ.mol^{-1} \quad (2)$$

The two reactions are both catalyzed by Ni NPs supported on Al_2O_3 and present several common intermediates and elementary steps (Fig. 4a), namely the CO_2-to-CO (or the reverse, for WGS) transformation.[9] However, because of very diverse thermodynamics, they are performed at significantly different temperatures, 300 and 650 °C for WGS and DRM, respectively, which could affect the preferred reaction mechanisms. In Al_2O_3-supported Ni NP catalysts, like in the majority of industrial NP catalysts, an oxide material is used to ensure the stability on stream, which provides additional interface sites on the metal/oxide boundary whose role in catalysis is often invoked and consequently highly debated (Fig. 4b).[10] Therefore, a detailed understanding of WGS and DRM mechanisms and especially the active sites (*e.g.* sites on the bare Ni NP vs. the Ni/Al_2O_3 interface) is desirable, but also challenging due to the complexity of the WGS and DRM reactions, displaying several elementary steps which may all take place on each of the available surface sites and are all potentially rate-determining.

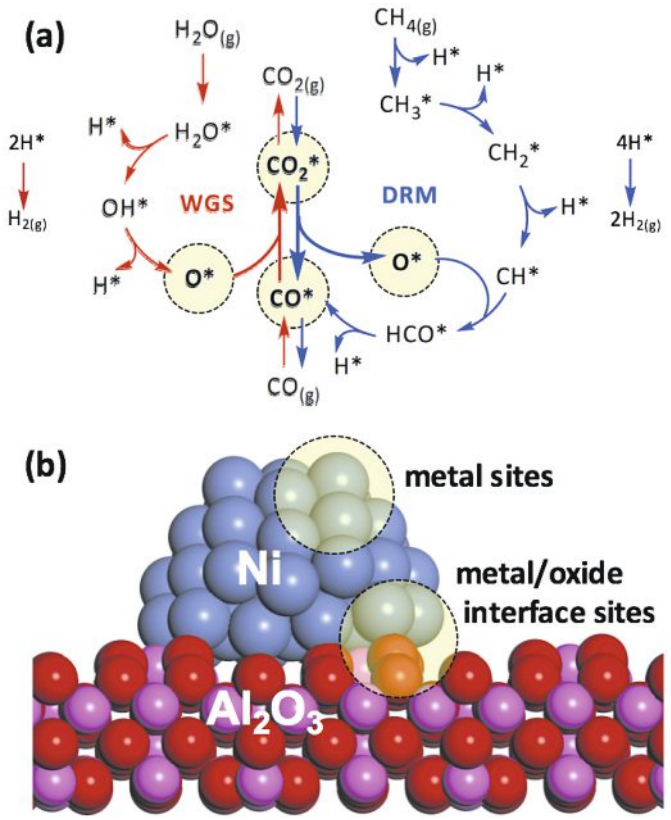

Fig. 4. (a) Representation of the main WGS (in red) and DRM (in blue) reaction mechanisms with common intermediates (CO_2*, CO* and O*) highlighted. (b) Schematic representation of nanoparticle (Ni) and interface (Ni/Al_2O_3) sites present in Al_2O_3-supported Ni NP catalysts. Ni, Al and O atoms are shown in blue, magenta and red, respectively, in (b). Adapted from ref. [13b].

2.1 *Evaluation of PES by DFT to Determine the Active Sites*

The interaction of several molecules involved in the WGS and DRM reaction networks with Ni vs. Ni/Al_2O_3 interface sites has been evaluated by DFT using Ni cluster models supported on Al_2O_3 surfaces. Interface sites were shown to strongly adsorb CO[11] or activate H_2, CH_4,[12] H_2O and CO_2[13] molecules with lower energy barriers compared to bare Ni sites located on the metal NP surface, presumably making the overall WGS and DRM easier at the interface. In particular, CO_2 direct activation, forming CO and O fragments in one elementary step, was shown to be much less energy-demanding on Ni/Al_2O_3 interface sites containing Lewis acidic Al atoms of the (110) γ-Al_2O_3 surface in the vicinity of the NP compared to bare metal sites on the Ni_{55} cluster model with *ca.* 1 nm diameter (PESs shown in Fig. 5a).[13a] Based on these results, both the WGS and DRM reactions could be proposed to occur preferentially *via* mechanisms operating on the metal/oxide interface. The PESs for the full catalytic cycles for the WGS and DRM reactions including the main proposed mechanisms were also evaluated on Ni and Ni/Al_2O_3 sites by DFT (Fig. 5b), from which the reaction free-energy span could be evaluated.[13b] Whereas the WGS reaction on Ni NP sites involves a free-energy span of 166 kJ.mol^{-1}, the reaction on the Ni/Al_2O_3 site is associated with 222 kJ.mol^{-1}. In the case of DRM, the free-energy spans correspond to 225 and 246 kJ.mol^{-1} for Ni NP and Ni/Al_2O_3 sites respectively. Therefore, based on the span model, the interface should be less active than the Ni sites. This is in contrast to the proposed role of the interface in favoring the WGS and DRM reactions based on the easier activation of CO_2 and H_2O on the interface compared to Ni as shown by the DFT-evaluated PESs, so one may wonder which of these contradictory interpretations is the correct one.

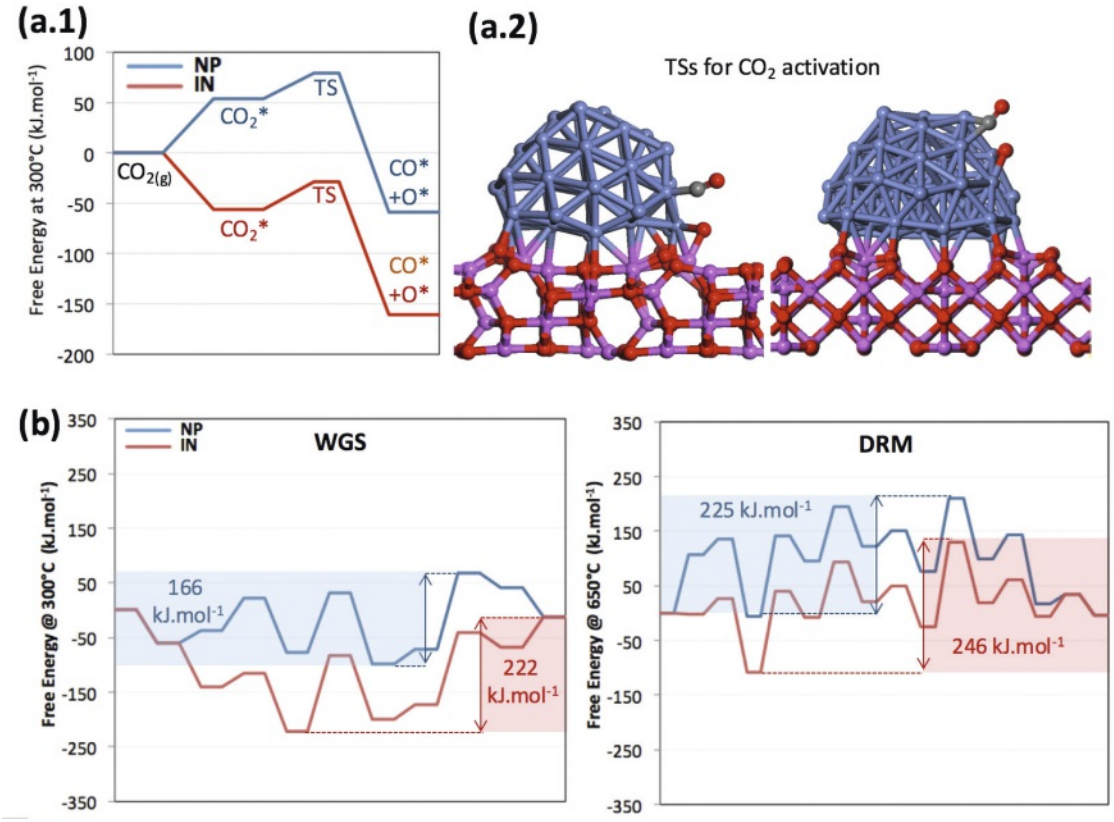

Fig. 5. Atomistic modeling: reaction energy profiles evaluated by DFT on nanoparticle (NP, in blue) and interface (IN, in red) sites present on Al_2O_3-supported Ni NP models. CO_2 adsorption and activation: (a.1) free energy profiles (at 300 °C) and (a.2) structure of the identified TSs. Ni, Al, O and C atoms are shown in blue, magenta, red and gray, respectively. (b) Free energy profiles evaluated at 300 and 650 °C for the full catalytic cycles of WGS and DRM, respectively, with indicated free energy spans. Adapted from refs [13b] and [13a].

2.2 *From PES to Formation Rates Using Microkinetic Modeling*

In order to have a better description of the catalytic process, including the effect of the different temperatures of WGS and DRM on reaction mechanisms and preference for metal vs. metal/oxide interface active sites as well as the complex reaction networks, the DFT data was used to construct a mean-field microkinetic model.[13b] Periodic DFT calculations were carried out with the VASP code,[14] using the PAW method (plane-wave basis set with pseudopotentials) and the PW91 exchange-correlation functional.[15] Kinetic modeling simulations were performed using the Chemkin® software[16] and a plug-flow reactor model. Within the mean-field approximation, the system is considered well-mixed, *i.e.* the reaction rates are calculated from the average coverage of surface species considering that they occupy adjacent sites on the surface of the catalyst allowing their reaction. The effect of the formation of separated domains of adsorbed species, which could decrease the probability of finding adsorbates in adjacent sites thus decreasing the reaction rate, is not modeled within this approximation. The kinetic model is dual-site and includes two different surface sites simultaneously, corresponding to the Ni NP surface to the Ni/Al_2O_3 interface. It contains six adsorption elementary steps describing the adsorption and desorption of reactants and product molecules on each of the sites as well as 27 surface reactions describing transformations on the Ni NP as well as on the Ni/Al_2O_3 interface. The set of surface reactions contains the most favorable WGS and DRM mechanisms on Ni identified by previous DFT studies.[9,17] The same model was used for the evaluation of both WGS and DRM reactions. Further computational details are available elsewhere.[13b]

From the steady-state rates of each individual reaction step of WGS and DRM reaction networks obtained from the microkinetic model (Fig. 6a), the main reaction pathway is associated with the Ni/Al_2O_3 interface for the WGS, whereas both Ni NP and Ni/Al_2O_3 sites are active for the DRM. The DRC analysis shows that the most RDSs of WGS and DRM are not the activation of reactants, but the dissociation of adsorbed hydroxyl groups (denoted OH*) and the CH* oxidation reaction with O*, respectively. The surface hydroxyl (OH*) and oxygen (O*) participating in these RDSs are much more available at the Ni/Al_2O_3 interface due to their favorable binding to Al_2O_3 Lewis acidic Al atoms on the perimeter of the Ni NP. During WGS at 300 °C, the NP is highly poisoned with adsorbed CO* and lacks OH* groups, so that the presence of interfacial OH* boosts the overall reaction rate at the interface. Conversely, during DRM at 650 °C, the coverage of adsorbed CO* on the Ni NP is rather low and O* is readily available within the metal, making the presence of interfacial O* not significant to the overall catalytic activity.

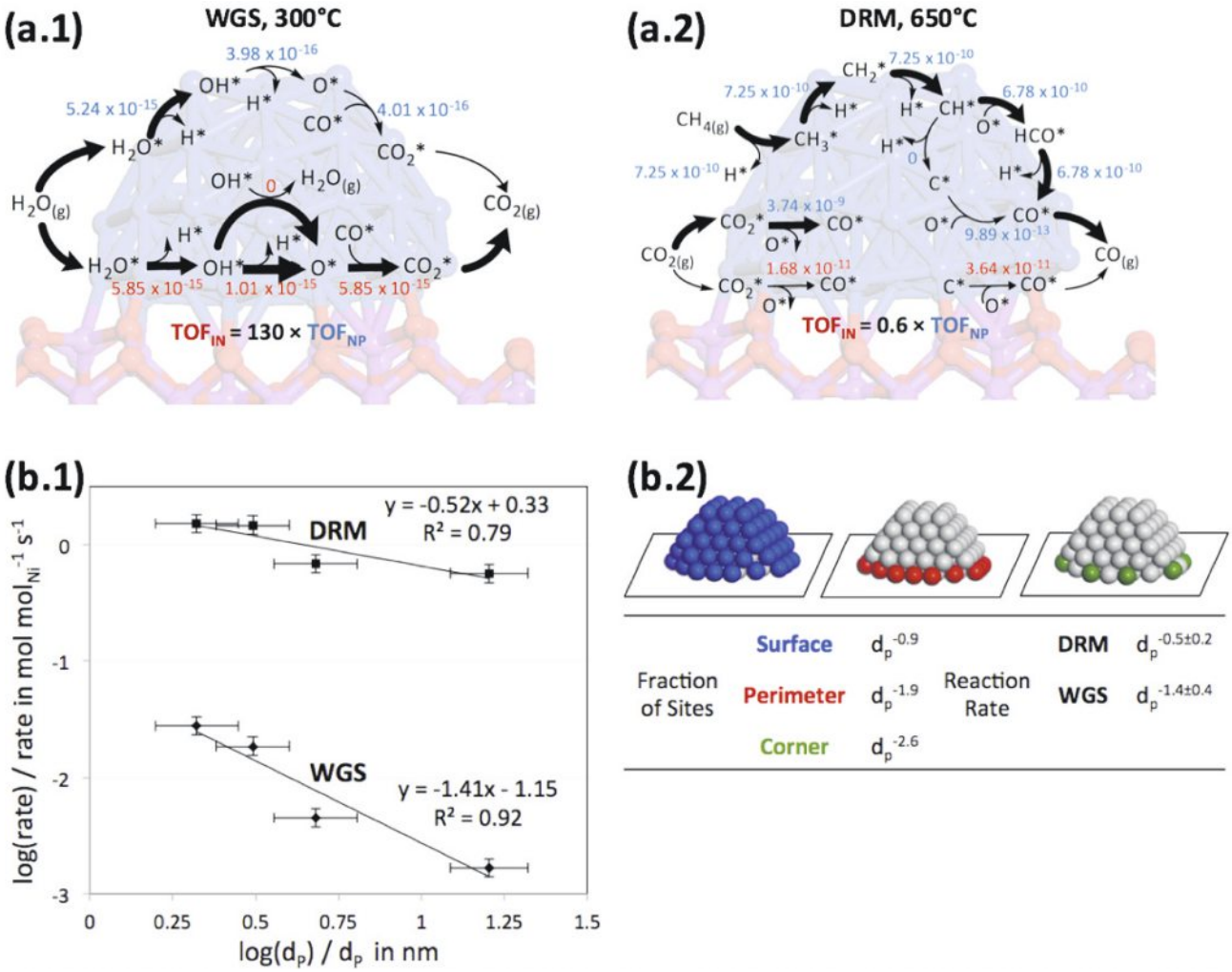

Fig. 6. (a) Kinetic modeling: net reaction rates for the main individual elementary steps of WGS and DRM reaction networks calculated with a DFT-derived dual-site (nanoparticle and interface) microkinetic model for Al_2O_3-supported Ni NP catalysts. Thick arrows indicate the preferred reaction channel. WGS reaction conditions: 300 °C, 1 bar, feed composition (molar fraction) 0.10 H_2O, 0.10 CO, 0.80 N_2. CO conversion: 10%. DRM reaction conditions: 650 °C, 1 bar, feed composition (molar fraction) 0.45 CH_4, 0.45 CO_2, 0.1 N_2; CH_4 conversion: 25%. (b) Experiments: (b.1) Measured reaction rates as a function of NP diameter (d_p) for Al_2O_3-supported Ni catalysts (logarithm scale) for WGS reaction at 300 °C (CO conversions between 12 and 15%) and DRM reaction at 650 °C (CH_4 conversions between 27 and 29 %). The experimental feed compositions are the same as those used in the kinetic model. (b.2) Evolution of rates and fraction of types of exposed metallic sites. Adapted from ref. [13b].

2.3 *Experimental Verification of Active Site Requirements*

If the active sites for WGS and DRM are different, as proposed by the microkinetic model, the reaction rates must depend on the proportion of interface sites present in Al_2O_3-supported Ni NP catalysts and thus on the NP size in a different manner for each of the reactions. This is because the evolution of the proportion of perimeter sites at the metal/support interface and surface sites with the NP diameter is different and decays as $\sim d_p^{-1.9}$ and $\sim d_p^{-0.9}$, for perimeter and surface sites, respectively.[10b,18] In fact, γ-Al_2O_3-supported Ni catalysts with different NP sizes behave differently in WGS and DRM reactions when the reaction rates are plotted against the average diameter of the catalyst particle (Fig. 6b.1).[19] The obtained dependence of WGS and DRM reaction rates on the NP diameter indicates that WGS is more efficiently promoted by sites residing in the Ni/Al_2O_3 perimeter whereas DRM is rather related to the total number of exposed metal atoms, since the evolution of the reaction rates with the diameter of the catalysts ($\sim d_p^{-0.5}$ and $\sim d_p^{-1.4}$ for WGS and DRM respectively) is similar to the evolution of the proportion of perimeter sites and surface sites with the NP diameter (Fig. 6b.2). Therefore, both experiments and microkinetic modelling confirm the different active site requirement in these reactions.

3. Perspectives and Conclusion

The multi-scale approach based in microkinetic models to understand catalytic processes catalyzed by metal NPs *via* the *ab initio* route presents several approximations that may be severe in some cases and which therefore should be further addressed. Firstly, since reaction rates depend exponentially on the enthalpy and entropy of surface reactions (Fig. 1b.1), small energy or entropy differences will produce large differences in rates. In this respect, the evaluation of energy with DFT may need to be done beyond the typically used generalized gradient approximation (GGA) for the exchange-correlation energy for improved accuracy (*e.g.* meta-GGA or hybrid functionals).[10a,20] Furthermore, when anharmonic effects or degrees of freedom other than the vibrational ones (translations, rotations) are relevant for adsorbate entropy, the commonly used harmonic approximation may introduce considerable errors.[21] Both these options represent, however, a sensible increase in the computational cost, which may be prohibitive depending on the size of the model system and complexity of the reaction network.

Another challenge is the representation of adsorbate–adsorbate interactions on highly-covered surfaces[22] and adsorbate gradients,[23] which can be tackled with the use of models beyond the mean-field approximation (*e.g.* kinetic Monte-Carlo). In particular, the energetics of a process occurring at high coverages may not be simply extrapolated from low-coverage calculations and may need to be more carefully evaluated in some cases (*e.g.* by using *ab initio* molecular dynamics methods).[24] Finally, the choice of model system is also a difficult task when numerous facets on metal NPs[25] or metal/oxide interfaces[26] are possible, not to mention NP size effects.[27]

In spite of such limitations, the use of first principles multi-scale models including kinetic analyses, which take into account the reaction conditions and the complexity of intricate reaction networks, has become a powerful tool to distinguish mechanisms and active sites operating in transition metal NPs, as illustrated here for the case of metal/oxide interfaces in the WGS and DRM reactions catalyzed by Ni NPs supported on Al_2O_3. Further developments of computational methods and realistic model systems ought to lead to a more comprehensive understanding of catalytic processes catalyzed by metal NPs *via* first principles.

Acknowledgements

ETH Zürich (research grant ETH42 14-1 and career seed grant SEED-21 16-2), the Holcim Foundation, and the Swiss competence center for energy research (SCCER heat and energy storage) are acknowledged for financial support. A. C.-V. acknowledges the Spanish MEC and the European Social Fund for a Ramon y Cajal research contract (RYC-2016-19930). We also acknowledge Prof. Christophe Copéret for fruitful discussions.

Received: January 15, 2019

[1] a) G. A. Somorjai, L. Yimin, 'Introduction to Surface Chemistry and Catalysis', Wiley, **1994**; b) J. P. Hindermann, G. J. Hutchings, A. Kiennemann, *Catal. Rev.* **1993**, *35*, 1.
[2] a) J. K. Norskov, T. Bligaard, J. Rossmeisl, C. H. Christensen, *Nat. Chem.* **2009**, *1*, 37; b) J. K. Nørskov, F. Abild-Pedersen, F. Studt, T. Bligaard, *Proc. Nat. Acad. Sci. USA* **2011**, *108*, 937.
[3] a) L. Falivene, S. M. Kozlov, L. Cavallo, *ACS Catal.* **2018**, *8*, 5637; b) S. Kozuch, S. Shaik, *Acc. Chem. Res.* **2011**, *44*, 101.
[4] a) J. A. Dumesic, 'The Microkinetics of heterogeneous catalysis', American Chemical Society, Washington, DC, USA, **1993**; b) S. Raimondeau, D. G. Vlachos, *Chem. Eng. J.* **2002**, *90*, 3; c) L. J. Broadbelt, R. Q. Snurr, *Appl. Catal., A*. **2000**, *200*, 23; d) P. Stoltze, *Prog. Surf. Sci*. **2000**, *65*, 65; e) D. G. Vlachos, *AlChE J.* **2012**, *58*, 1314; f) M. Salciccioli, M. Stamatakis, S. Caratzoulas, D. G. Vlachos, *Chem. Eng. Sci.* **2011**, *66*, 4319.
[5] H. S. Fogler, 'Elements of chemical reaction engineering', Prentice-Hall, **1986**.
[6] a) C. T. Campbell, *ACS Catal.* **2017**, *7*, 2770; b) C. T. Campbell, *Top. Catal.* **1994**, *1*, 353; c) C. T. Campbell, *J. Catal.* **2001**, *204*, 520; d) C. Stegelmann, A. Andreasen, C. T. Campbell, *J. Am. Chem. Soc.* **2009**, *131*, 8077.
[7] C. Ratnasamy, J. P. Wagner, *Cat. Rev.* **2009**, *51*, 325.
[8] a) M. De Falco, G. Iaquaniello, G. Centi, 'CO_2: A Valuable Source of Carbon', Springer London ; Imprint: Springer, **2013**; b) D. Pakhare, J. Spivey, *Chem. Soc. Rev.* **2014**, *43*, 7813.
[9] L. Foppa, M.-C. Silaghi, K. Larmier, A. Comas-Vives, *J. Catal*. **2016**, *343*, 196.
[10] a) Z.-J. Zhao, Z. Li, Y. Cui, H. Zhu, W. F. Schneider, W. N. Delgass, F. Ribeiro, J. Greeley, *J. Catal.* **2017**, *345*, 157; b) M. Shekhar, J. Wang, W.-S. Lee, W. D. Williams, S. M. Kim, E. A. Stach, J. T. Miller, W. N. Delgass, F. H. Ribeiro, *J. Am. Chem. Soc*. **2012**, *134*, 4700; c) S. Aranifard, S. C. Ammal, A. Heyden, *J. Catal*. **2014**, *309*, 314; d) S. C. Ammal, A. Heyden, *J. Catal.* **2013**, *306*, 78; e) J. H. Bitter, K. Seshan, J. A. Lercher, *J. Catal*. **1997**, *171*, 279; f) J. H. Bitter, K. Seshan, J. A. Lercher, *J. Catal.* **1998**, *176*, 93; g) Z. Liu, D. C. Grinter, P. G. Lustemberg, T.-D. Nguyen-Phan, Y. Zhou, S. Luo, I. Waluyo, E. J. Crumlin, D. J. Stacchiola, J. Zhou, J. Carrasco, H. F. Busnengo, M. V. Ganduglia-Pirovano, S. D. Senanayake, J. A. Rodriguez, *Angew. Chem.* **2016**, *128*, 7581; h) P. G. Lustemberg, P. J. Ramírez, Z. Liu, R. A. Gutiérrez, D. G. Grinter, J. Carrasco, S. D. Senanayake, J. A. Rodriguez, M. V. Ganduglia-Pirovano, *ACS Catal.* **2016**, *6*, 8184.
[11] a) G. Pacchioni, N. Rösch, *Surf. Sci.* **1994**, *306*, 169; b) L. G. V. Briquet, C. R. A. Catlow, S. A. French, *J. Phys. Chem. C* **2010**, *114*, 22155.
[12] J. Li, E. Croiset, L. Ricardez-Sandoval, *J. Phys. Chem. C* **2013**, *117*, 16907.
[13] a) M.-C. Silaghi, A. Comas-Vives, C. Copéret, *ACS Catal.* **2016**, *6*, 4501; b) L. Foppa, T. Margossian, S. M. Kim, C. Müller, C. Copéret, K. Larmier, A. Comas-Vives, *J. Am. Chem. Soc*. **2017**, *139*, 17128.
[14] a) G. Kresse, J. Hafner, *Phys. Rev. B* **1994**, *49*, 14251; b) G. Kresse, J. Hafner, *Phys. Rev. B* **1993**, *47*, 558; c) G. Kresse, J. Furthmüller, *Comput. Mater. Sci.* **1996**, *6*, 15.
[15] J. P. Perdew, J. A. Chevary, S. H. Vosko, K. A. Jackson, M. R. Pederson, D. J. Singh, C. Fiolhais, *Phys. Rev. B* **1992**, *46*, 6671.
[16] 'Chemkin-Pro 15131', Reaction Design, San Diego, **2013**.
[17] C. Fan, Y.-A. Zhu, M.-L. Yang, Z.-J. Sui, X.-G. Zhou, D. Chen, *Ind. Eng. Chem. Res.* **2015**, *54*, 5901.
[18] M. Cargnello, V. V. T. Doan-Nguyen, T. R. Gordon, R. E. Diaz, E. A. Stach, R. J. Gorte, P. Fornasiero, C. B. Murray, *Science* **2013**, *341*, 771.
[19] T. Margossian, K. Larmier, S. M. Kim, F. Krumeich, A. Fedorov, P. Chen, C. R. Müller, C. Copéret, *J. Am. Chem. Soc*. **2017**, *139*, 6919.
[20] S. Mallikarjun Sharada, T. Bligaard, A. C. Luntz, G.-J. Kroes, J. K. Nørskov, *J. Phys. Chem. C* **2017**, *121*, 19807.
[21] a) M. Jørgensen, H. Grönbeck, *J. Phys. Chem. C* **2017**, *121*, 7199; b) G. Piccini, M. Alessio, J. Sauer, *Angew. Chem. Int. Ed.* **2016**, *55*, 5235; c) L. H. Sprowl, C. T. Campbell, L. Árnadóttir, *J. Phys. Chem. C* **2016**, *120*, 9719; d) A. Bajpai, P. Mehta, K. Frey, A. M. Lehmer, W. F. Schneider, *ACS Catal.* **2018**, *8*, 1945.
[22] a) M. Zhou, B. Liu, *Ind. Eng. Chem. Res.* **2017**, *56*, 5813; b) A. C. Lausche, A. J. Medford, T. S. Khan, Y. Xu, T. Bligaard, F. Abild-Pedersen, J. K. Nørskov, F. Studt, *J. Catal.* **2013**, *307*, 275.
[23] M. Stamatakis, D. G. Vlachos, *ACS Catal.* **2012**, *2*, 2648.
[24] L. Foppa, M. Iannuzzi, C. Copéret, A. Comas-Vives, *ACS Catal.* **2018**, *8*, 6983.
[25] K. Reuter, C. P. Plaisance, H. Oberhofer, M. Andersen, *J. Chem. Phys.* **2017**, *146*, 040901.
[26] P. Mehta, J. Greeley, W. N. Delgass, W. F. Schneider, A*CS Catal.* **2017**, *7*, 4707.
[27] L. Foppa, C. Copéret, A. Comas-Vives, *J. Am. Chem. Soc*. **2016**, *138*, 16655.